A spatiotemporally regulated drug delivery system with stage-specific thermosensitive gelation and photothermally triggered release for localized tumor therapy

Shuyue Chang[a†], Jinming Wei [a†], Yike Fu[a,b†], Zijie Lu[c], Weiren Liang[d], Jun Luo[d*], Chao Fang[c*], Xiang Li[a*]

[a]*State Key Laboratory of Silicon and Advanced Semiconductor Materials, School of Materials Science and Engineering, Zhejiang University, Hangzhou 310058, China*

[b]*ZJU-Hangzhou Global Scientific and Technological Innovation Center, Zhejiang University, Hangzhou 311215, China*

[c] *iBioMat Hi-Tech (Zhejiang) Co., Ltd., 3F, Bldg C, Future Health Science and Innovation Park, 2959 Yuhangtang Rd, Hangzhou 311121, China*

[d]*Zhejiang Cancer Hospital, Hangzhou Institute of Medicine (HIM), Chinese Academy of Sciences, Zhejiang, Hangzhou 310022, China*

[†]These authors contributed equally to this work;

[*] **Correspondence**: bjy0927@163.com (J.L); 11626007@zju.edu.cn (C.F); xiang.li@zju.edu.cn (X.L)

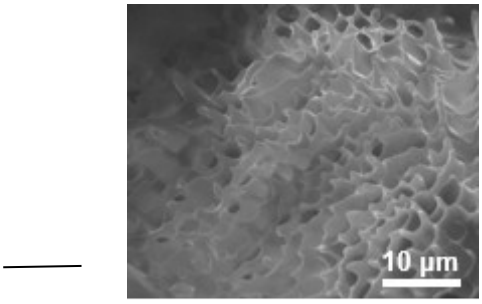

Figure S1. SEM images of P(NIPAM-co-AM) nanogel.

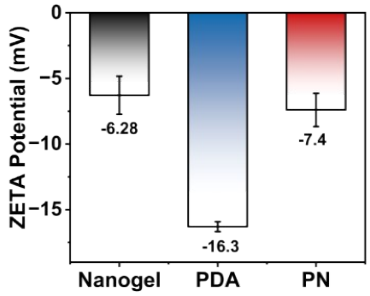

Figure S2. Zeta potentials of P(NIPAAm-co-AM) nanogels, PDA and PN.

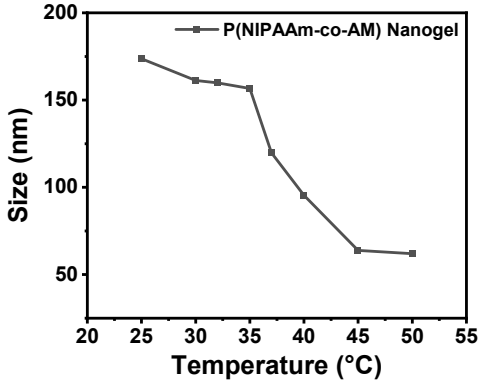

Figure S3. Size variations of P(NIPAAm-co-AM) nanogel with temperature.

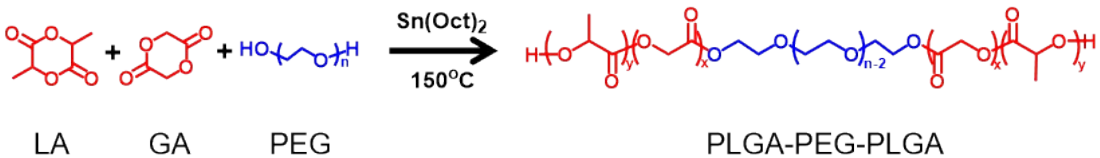

Figure S4. Schematic diagram of the synthesis route of PLGA-PEG-PLGA block copolymers.

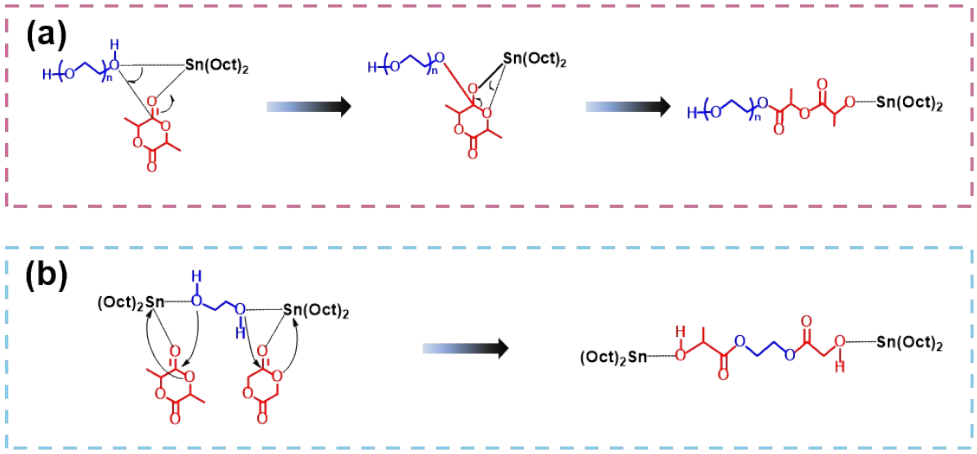

Figure S5. Schematic diagram of the synthesis mechanism of PLGA-PEG-PLGA block copolymers.

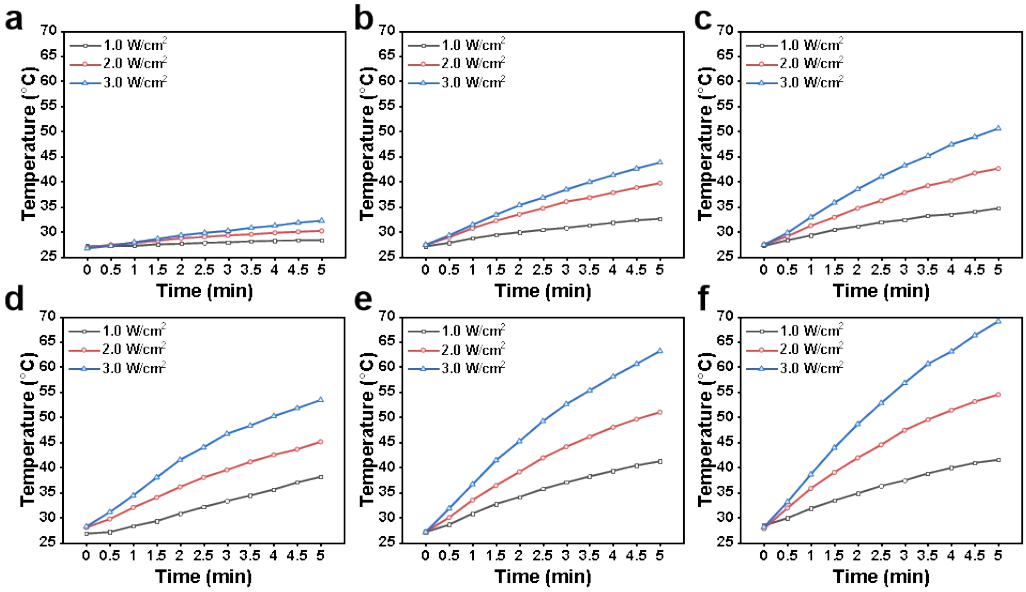

Figure S6. Heating curves of PDA@P(NIPAM-co-AM) solutions at different concentrations under NIR irradiation (808 nm, 5 min): (a) 0 μg/mL, (b) 50 μg/mL, (c) 75 μg/mL, (d) 100 μg/mL, (e) 150 μg/mL and (f) 200 μg/mL.

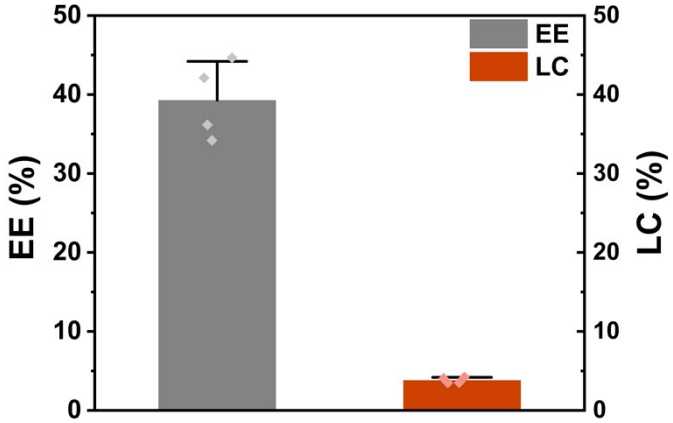

Figure S7. When the ratio of DOX to PN in the feeding quality is 1:10, the drug loading rate and encapsulation efficiency of PN.

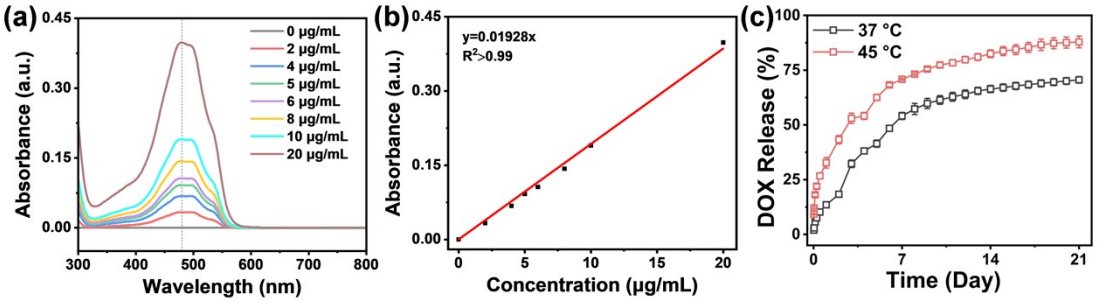

(d)

Mathematical models		37 ℃	45 ℃
Zero-order	R^2	0.9576	0.8364
First-order	R^2	0.6839	0.8181
Higuchi	R^2	0.9792	0.9696
Ritger-Peppas	R^2	0.9776	0.9949
	n	0.4951	0.3227

Figure S8. (a) UV-Vis spectra of DOX solutions at different concentrations. (b) Standard curve of DOX loading. (c) Drug release curves of DPNP at different temperatures. (d) Mathematical model fitting correlation coefficients for DOX release curves of DPNP at 37 °C and 45 °C.

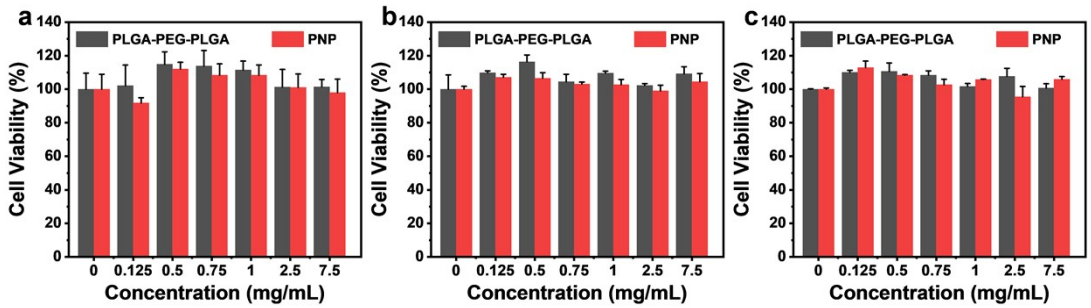

Figure S9. (a) Cell viabilities of L929 cells treated with different concentrations of PLGA-PEG-PLGA and PNP for 48 h. Cell viabilities of AML 12 cells treated with different concentrations of PLGA-PEG-PLGA and PNP for (b) 24 h and (c) 48 h.

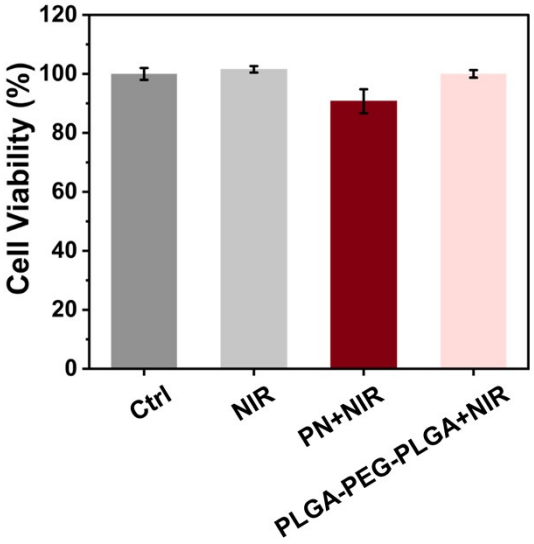

Figure S10. Cell viability of 4T1 cells after different treatments (NIR, PN + NIR, and PLGA-PEG-PLGA + NIR).

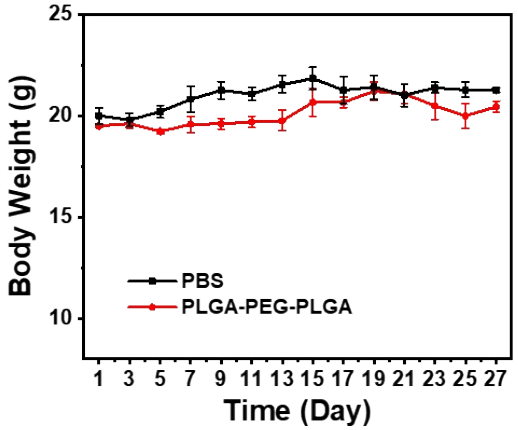

Figure S11. Body weight curves of mice in the control group and the group subcutaneously injected with PLGA-PEG-PLGA hydrogel within 27 days (n=3, mean±SD).

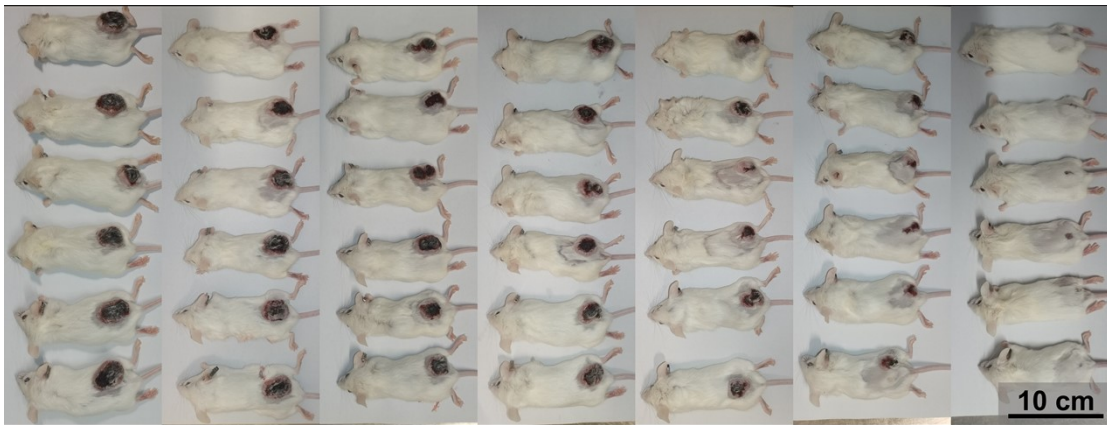

Figure S12. Photographs of treated mice on the 21st day after different treatments.

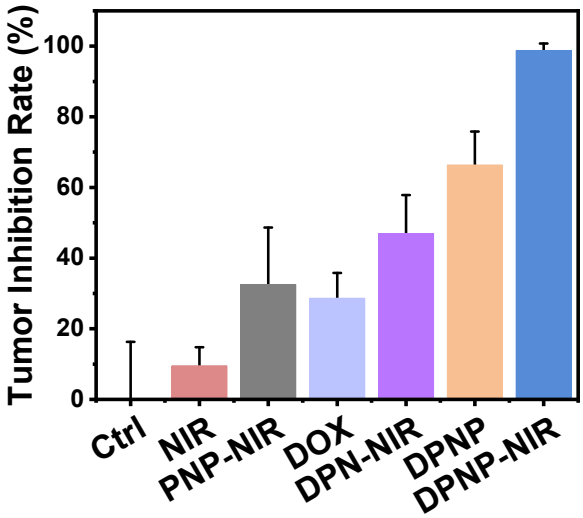

Figure S13. Comparison of tumor inhibition rate in various treatment groups. n=6, mean ± SD.

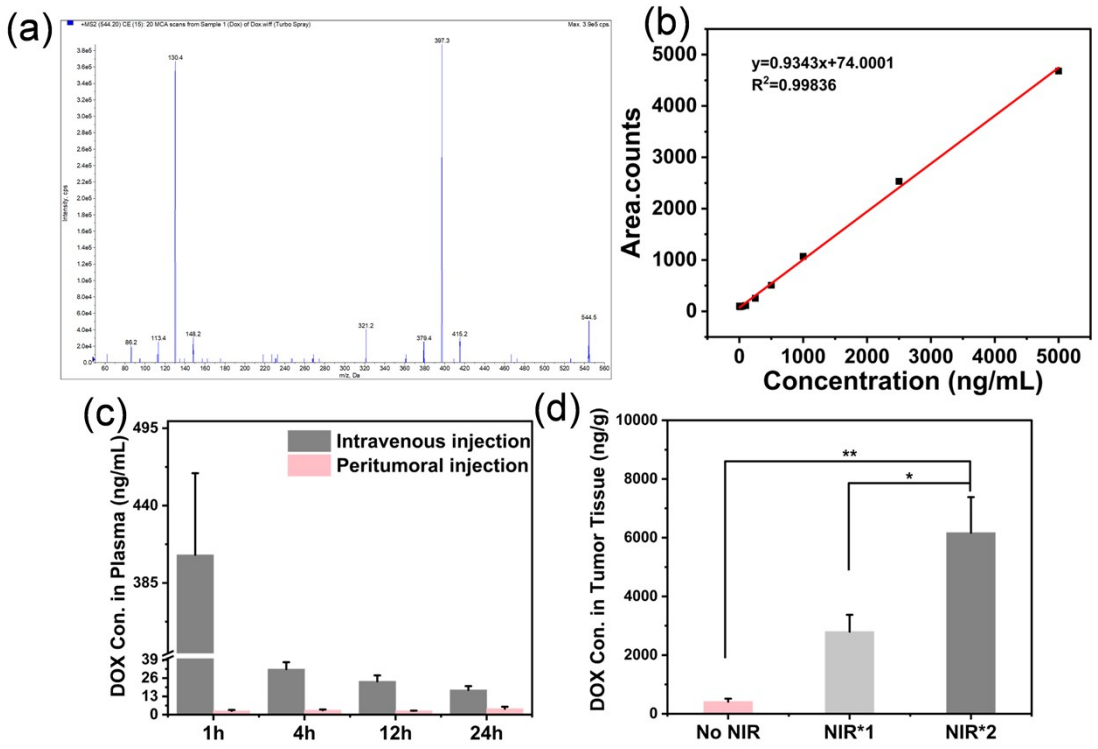

Figure S14 (a) The mass spectrum diagram of DOX. (b) Standard curve of DOX loading. (c) The blood drug concentration after intravenous injection of DOX and peritumoral injection of DPNP. (d) The concentration of DOX in tumor tissues after different treatments.

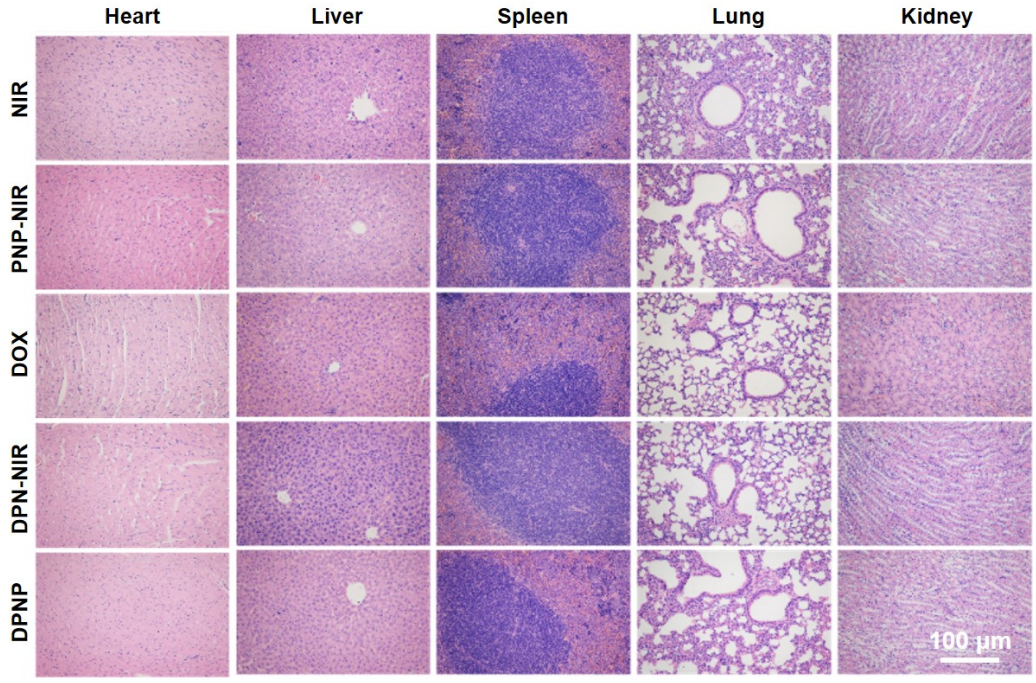

Figure S15. H&E staining images of major organs from mice in different treatment groups at day 21.

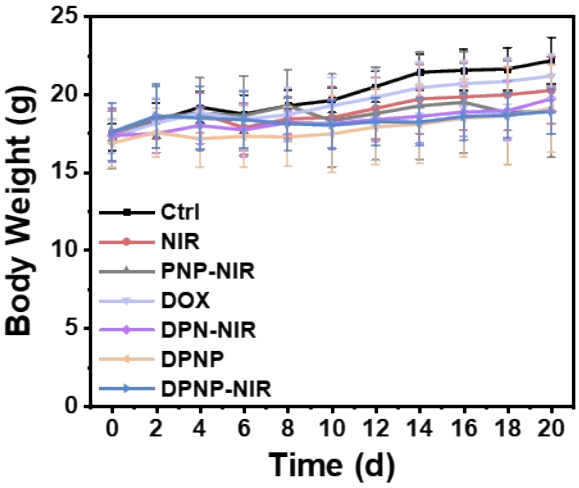

Figure S16. The profiles of body weights of mice in various treatment groups.